Journal of Cleaner Production 234 (2019) 559–567

Contents lists available at ScienceDirect

Journal of Cleaner Production

journal homepage: www.elsevier.com/locate/jclepro

Experimental study of high-performance autoclaved aerated concrete produced with recycled wood fibre and rubber powder

Tingshu He [a], Rongsheng Xu [a, *], Yongqi Da [a], Renhe Yang [a], Chang Chen [a, **], Yang Liu [b]

[a] School of Materials Science and Engineering, Xi'an University of Architecture & Technology, Xi'an, 710055, China
[b] Shanxi NITYA New Materials Technology Co. Ltd, Xi'an, 710055, China

ARTICLE INFO

Article history:
Received 20 December 2018
Received in revised form
20 June 2019
Accepted 23 June 2019
Available online 24 June 2019

Handling Editor: M.T. Moreira

Keywords:
Recycled rubber powder
Recycled wood fibre
Autoclaved aerated concrete
Thermal conductivity
Mechanical properties

ABSTRACT

The brittleness and low fracture toughness of autoclaved aerated concrete (AAC) could be improved by fibres, but the deterioration of its thermal insulation performance are commonly observed. In this study, different combinations of recycled wood fibre and rubber powder were added in AAC to improve its performance and reduce the negative environmental impacts of solid waste. In addition to the fluidity of slurry, the physical, mechanical and thermal properties of AAC were systematically investigated, together with the phase components and microstructure images. AAC with relative high mechanical strengths and excellent thermal insulation performances could be obtained because of the reinforcement of wood fibre and the gas introduced by rubber powder. The scanning electron microscopy (SEM) and X-ray diffraction (XRD) analyses revealed that the positive effects of wood fibre and rubber powder were the results of physical interactions.

1. Introduction

Recently, energy conservation with respect to buildings has become a growing concern (Kočí et al., 2013). In China, 20.6% of the total energy and 19.0% of the total carbon emission have been consumed by building in 2016 (China Building Energy Saving Technic Association, 2019). A series of energy codes for buildings has implemented to effectively reduce building energy consumption. To achieve the goal of 65% building energy conservation, the internal-external insulation measure and wall materials with good thermal insulation performance are adopted (Wang et al., 2019). Autoclaved aerated concrete (AAC) has been reported to be the only wall material meets the Chinese national standard requirement of the energy conservation for buildings (He et al., 2018).

AAC is usually the mixture of quartz powder (or fly ash), cement, lime, gypsum, water and small quantities of aluminum powder, which is hardened and strengthened under pressurized steam (Israngkura Na Ayudhya, 2016; Schreiner et al., 2018). Compared with ordinary concrete, AAC has the more excellent thermal insulation properties and the lower density (Asadi et al., 2018; Ma et al., 2016; Yuan et al., 2017). However, AAC products also have some drawbacks, such as high brittleness and low mechanical strength, which limits their commercial applications (Cong et al., 2016; Ferretti et al., 2015; Koudelka et al., 2015). Moreover, recent trends have focused on utilizing industrial wastes to produce high-performance AAC, that is, AAC with high volume stability, high mechanical strength, and excellent thermal insulation properties (El-Didamony et al., 2019).

Studies have shown that adding fibre was a simple and effective way to obtain AAC with relatively high volume stability and mechanical strength (Bonakdar et al., 2013; Laukaitis et al., 2012; Pehlivanlı et al., 2016). However, not all fibres are suitable for addition to AAC owing to the special preparation process used for AAC, such as polymer fibre may melt under the high temperature, carbon fibre cannot easy to disperse in AAC slurry. (Noumowe and Research, 2005; Yang et al., 2017). Several research projects have been carried out to use the natural fibre in cement-based materials. About 20% increase in strength and an obvious improvement in load-carrying capacity of concrete cylinder are obtained with the additions of the coir fibre and sisal fibre (Krishna et al., 2018).

Wood is a natural material and used worldwide as a construction material for both long-term and temporary use (Faraca et al., 2019). A significant amount of wood waste is generated because

* Corresponding author.
** Corresponding author.
E-mail address: xrslove@sohu.com (R. Xu).

https://doi.org/10.1016/j.jclepro.2019.06.276
0959-6526/

of rapid urbanisation and industrialisation (Souza et al., 2018). For instance, thousands of tons of wood waste are produced from construction, furniture manufacture, and other activities in China. Historically, this wood waste is not classified and is usually used as fuel or directly discarded, causing serious environmental concerns and health issues (Wang et al., 2017). However, wood waste is considered a recyclable and renewable resource, so transforming wood waste into an innovative upcycling option is necessary. As the most widely used natural organic fibre, it has been used successfully in cement-based material because of its low density and cost, high mechanical properties, excellent dispersion and thermal properties (Blankenhorn et al., 2001; Nasser et al., 2016; Quiroga et al., 2016; Usman et al., 2018). In addition, with respect to the sustainability strategy, the use of wood fibre produced from wood waste has a positive environmental impact (Hossain and Poon, 2018; Wang et al., 2018).

Unfortunately, the thermal conductivity of AAC reduces by more than 15% while fibres are added (Pehlivanlı et al., 2016). Because of its unique pore structure, AAC cannot have relatively high mechanical strength and relatively low thermal conductivity at same time. The pore structure of AAC changes significantly when fibres are added. As the porosity of AAC decreases, its mechanical properties increase but its thermal conductivity also increases. Moreover, the relatively high thermal conductivity of fibres and the negative effect of the thermal bridge caused by the fibre additives could directly affect the thermal insulation property of AAC (Xargay et al., 2018). To achieve a high insulation level, several studies have been carried out to improve the thermal insulation property of AAC using various phase-change materials, such as kalium carbonate, octadecanoic acid, and phase-change paraffin (Cao et al., 2017; Kahwaji et al., 2018; Li et al., 2017). However, these phase-change materials substantially increase the cost of AAC, which restricts its popularisation.

In recent decades, the production of rubber has increased significantly to satisfy the global demands for rubber products (Rahimi R et al., 2016). The production of rubber increased by nearly 10 million metric tons from 2000 to 2016 (Zhang et al., 2019). More than 1.5 billion tyres are manufactured worldwide and millions of tyres are discarded per annum (Ashish, 2018). Disposal of waste tyres has become a non-negligible environmental issue. Despite the massive effort to recycle waste tyres, the majority are still dumped in a landfill or burnt, which presents a serious threat to the ecological environment (Dobrotă and Dobrotă, 2018; Hijazi et al., 2018). Nevertheless, waste tyres could be seen as a valuable resource and spur researchers to develop new ways to eliminate this threat. The recycling of waste tyre rubber into construction materials for civil engineering has been investigated extensively the past few years. (Ramdani et al., 2019). Rubber powder has been used as filler in road construction (Sheng et al., 2017) and as a coarse or fine aggregate in cementitious materials like mortar and concrete (Cheng et al., 2017; Ismail et al., 2018; Long et al., 2018). However, rubber powder does decrease the mechanical strength of concrete because of the low stiffness of rubber and the poor bond between rubber powder and the cement matrix. Nonetheless, when recycled rubber is added to concrete, desirable improvements such as a decrease in the unit weight, improved ductility and toughness, and an increase in the cracking resistance are obtained. (Sienkiewicz et al., 2017; Thomas et al., 2016). In addition, the air content of rubber-reinforced concrete is slightly higher than that of reference mixtures without rubber (Aslani et al., 2018). Rubber powder introduces a small amount of gas into the mixture during the mixing process (Zhu et al., 2011), which has a favourable impact on the thermal insulation property of mixture.

The aim of this study was to utilise recycled rubber powder and wood fibre to produce AAC with excellent mechanical properties and thermal insulation performance. On the basis of the mixture ratios of commercial AAC, different contents of wood fibre and rubber powder were added to the mixtures to prepare AAC for testing. The effects of the rubber powder and wood fibre on the fluidity of the slurry, pore structure, and bulk density were evaluated. In addition, the mechanical properties of compressive strength and flexural strength were tested, and the optimal wood fibre content was determined. Then, the effects of rubber powder on thermal conductivity and energy-saving aspect were tested. Finally, the microstructure and phase components of the tested specimens were investigated using scanning electron microscopy (SEM) and X-ray diffraction (XRD), respectively.

2. Material and methods

2.1. Materials

The main raw materials used were cement, lime, gypsum and glass tailing sand (quartz sand powder). All raw materials used in the experiment were from the same batch to ensure the stability of the chemical composition of the specimens. Table 1 presents the chemical compositions of the main raw materials. The cementitious material used in this study was commercial Ordinary Portland Cement (OPC) 42.5R provided by Shanxi Jidong Cement Co. Ltd (Baoji, Shanxi province, China). To improve the pozzolanic activity, a laboratory mill was used to grind the glass tailing sand (provided by China Material Energy Saving New Materials Co, Ltd, Yichang, Hubei province, China) to quartz powder with a specific surface area of 5000 cm^2/g. Commercially available aluminium powder with the specific surface area of 7500 cm^2/g was provided by Shanxi NITYA New Materials Technology Co. Ltd (Xian, Shanxi Province, China).

Research has revealed that fibres with an average length of 2–6 mm could significantly enhance the mechanical properties of AAC (Laukaitis et al., 2009). Accordingly, wood fibre produced from pine waste, with an average length of 3.5 mm was used (Xian Chaomai Engineering Fiber Co. Ltd, Xian, Shanxi Province, China). The diameter and tensile strength of wood fibre were 38 ± 5 μm and 450–700 MPa, respectively. Rubber powder produced from tyre waste was provided by Hengshui Zehao Rubber Chemical Co. Ltd (Hengshui City, Hebei Province, China). To give full play of the air entraining function of rubber powder, the fineness of rubber powder was less than 180 mesh (0.088 mm).

2.2. Specimens preparation

In this study, B05 bulk density class AAC was used (the product number indicated a nominal apparent density of 500 kg/m^3). The initial mixture ratios of B05 bulk density class AAC were provided by Shanxi NITYA New Materials Technology Co. Ltd (Xian, Shanxi province, China). The content of sand, cement, lime, gypsum and aluminium powder were 59.0 wt%, 20.0 wt%, 2.0 wt% and 0.085 wt %, respectively. And the water/solid ratio was 0.60. All combinations of wood fibre and rubber powder were based on first improving the brittleness and fracture toughness of AAC, and then enhancing its thermal insulation performance. It has been reported that a high

Table 1
Chemical compositions of the main raw materials used (in mass%).

Raw material	SiO_2	Al_2O_3	Fe_2O_3	CaO	MgO	LOI [a]
Quartz powder	86.41	5.4	0.36	1.95	0.47	4.51
Cement	20.78	6.05	4.62	63.03	1.15	4.79
Lime	3.74	1.81	0.69	90.46	2.26	1.04

[a] LOI: Loss on ignition at 950 °C.

amount of fibre additive can lead to the deterioration of the mechanical strength of AAC (Pehlivanlı et al., 2015). Therefore, the wood fibre contents used in our study were 0.1%, 0.2%, 0.3%, 0.4%, and 0.5% of the total weight of the dry mixes. Moreover, even though the rubber powder content was as low as 5.0% in some studies, a negative impact of rubber powder on the mechanical properties of cement-based materials was still observed (Sofi, 2018; Thomas and Gupta, 2016). To ensure the mechanical performance of the AAC, the rubber powder contents adopted for this study were 0.5%, 1.0%, 1.5%, 2.0%, and 2.5% of the total weight of the dry mixes.

The procedures used in previous studies for preparing fibre-reinforced AAC (Laukaitis et al., 2009; Pehlivanlı et al., 2016), were the basis of the following procedure for preparing AAC specimens in this study.

(1) Wood fibre and rubber powder were mixed with quartz sand powder for 300 s.
(2) The other raw solid materials were added and the mixture was mixed for 150 s with water preheated to 50 °C.
(3) Aluminium powder was added and mixed with the slurry for another 40 s.
(4) The forming mixture was poured into warm $500 \times 500 \times 800\ mm^3$ serving moulds and then allowed to expand and harden at 50 °C for 3 h.
(5) Specimens were put into an autoclave at 190 °C and steamed under pressure for 12 h.

2.3. Testing procedure

The properties of the specimens were determined in the laboratory with temperature and relative humidity of 20 ± 2 °C and 60 ± 5%, respectively.

2.3.1. Fluidity of the slurry

A cylindrical mould ($40 \times 100\ mm^2$) was placed at the centre of a clean glass plate and filled with slurry at a constant speed. The expansion diameters in two vertical directions were measured with a ruler and their average value was adopted.

2.3.2. Bulk density and pore structure

For the bulk density test, three AAC specimens, exactly $100 \times 100 \times 100\ mm^3$, were oven-dried at 60 ± 5 °C for 24 h, then at 80 ± 5 °C for 24 h, and finally at 105 ± 5 °C until a constant weight was achieved. The volume and mass of the specimens were determined and used to calculate the volume density as follows:

$$\rho = m/v \quad (1)$$

where $\rho$is the volume density, m is the mass, and v is the volume of a specimen.

The matrix density ρ_1 was measured using pycnometry in the dry state. Thus, the porosity φ was determined as follows:

$$\varphi = 1 - \rho/\rho_1 \quad (2)$$

The surface macropores of a specimen were investigated using the following procedure: i) A colour photograph was taken on the specimen's surface with $100 \times 100\ mm^2$ area with a SONY DSC-WX350 camera (18.2 million pixels). ii) A screenshot of a $25 \times 25\ mm^2$ area on the image was obtained. iii) The screenshot was binarised using the binarisation function of MATLAB 2016a with a threshold of 150. iv) The macropores and AAC matrix were displayed in white and black, respectively. v) At last, the average pore diameter value was calculated with the software.

2.3.3. Mechanical properties

The compressive strength and flexural strength of the reinforced AAC specimens were tested according to the Chinese Standard GB 11968–2008 "Test methods of autoclaved aerated concrete". The compressive strength specimens were $100 \times 100 \times 100\ mm^3$ and the flexural strength specimens were $100 \times 100 \times 400\ mm^3$. The mechanical properties were tested on three samples with a moisture content of 8–12% using a powerful electromechanical testing machine (TYE-300D, Wuxi Jianyi Instrument & Machinery Co. Ltd).

2.3.4. Thermal property

A $300 \times 300 \times 30\text{-}mm^3$ specimen was dried in a stove at 65 ± 5 °C before undergoing thermal conductivity testing following the Chinese Standard GB/T 10294–2008 "Thermal insulation – Determination of steady-state thermal resistance and related properties – Guarded hot plated apparatus", using a thermal conductivity measurement instrument (PDR-3030B, Shenyang Weite General Technology Development Co. Ltd, Shenyang, Liaoning, China).

To investigate the stored-heat release property of AAC, we used the thermal system presented in Fig. 1. Before testing, a $400 \times 400 \times 40\text{-}mm^3$ specimen was dried at 65 ± 5 °C until a constant mass was achieved. The testing procedure was as follows: First, the specimen was installed and the testing system was debugged. Then, the iodide-tungsten lamp heat source was turned on. Finally, the heat source was turned off for natural cooling when the outer surface temperature was stable. The temperature data were collected every 20 min.

2.3.5. XRD and SEM

The microstructure of the test samples was observed by SEM using a Nova Nano SEM200 high-resolution scanning electron microscope (FEI, Thermo Fisher Scientific, Waltham, MA, USA). The mineral phases of the samples were observed by X-ray diffraction (XRD) analysis using a X'Pert Pro diffractometer (Malvern Panalytical, Malvern, UK).

3. Results and discussion

For convenience, the specimens were encoded as W*x*-*y* for this paper. *x* and *y* stand for the wood fibre content and the rubber powder content, respectively. For example, the AAC specimens with 0.4% wood fibre content and 1.0% rubber powder content is encoded as W0.4–1.0, and the specimen with no rubber powder and wood fibre is encoded as W0-0 (control specimen).

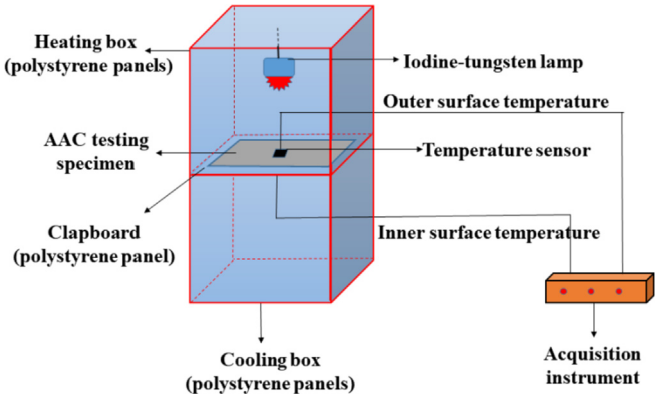

Fig. 1. Schematic diagram of the thermal insulation performance testing system.

3.1. Fluidity of slurry

Low fluidity can cause the AAC to perform poorly. According to the empirical data for this technological parameter obtained during AAC production, the target fluidity of 330 ± 35 mm should be achieved to ensure that the AAC has the properties of the B05 bulk density class (Straub et al., 2015). As presented in Fig. 2, the fluidity of slurry (the standard deviation ≤ 15 mm, less than 5% of the average fluidity) increased when the rubber powder content varied from 0 to 2.5%. Compared with W0-0 and W0.4–0, the fluidity values increased by 4.6% for W0-2.5 and 4.8% for W0.4–2.5, respectively. Rubber powders may act as glass microballoons in the slurry, which could reduce its viscosity and improve its fluidity.

On the other hand, the fluidity of the slurry decreased as the wood fibre content increased from 0% to 0.5%. Compared with W0-0 (control slurry without fiber and rubber powder), the fluidity value of W0.5-0 decreased by 21 mm. Because of the combined effects of the rough surface, flatness and bendability of wood fibre, the friction between the wood fibre and the slurry was relatively large, impairing the flow of the slurry. However, the fluidity of the W0.5-0 slurry still satisfied the technological parameter.

3.2. Bulk density and porosity

Bulk density is qualified by the mixing ratios and properties of the raw materials in AAC. The physical, thermal, and mechanical properties of AAC are closely related to the bulk density. Fig. 3 presents the relationship between bulk density (the standard deviation ≤ 8 kg/m^3, less than 2% of the average bulk density) and rubber powder content. It was found that the minimum bulk density was obtained while the rubber powder content was 0.1%. In addition, the bulk density increased along with the increase of wood fibre content. Thus, the minimum bulk density of 490 kg/m^3 was observed in specimen W0-1.0.

The properties of AAC depend significantly on its porosity and pore structure (distribution, size, and shape). Table 2 shows that the change in porosity with the change in rubber powder content had the same tendency as that with volume density. The porosity increased with the increase in rubber powder content owing to gas introduced by the rubber powder. Moreover, the porosity decreased as the wood fibre content changed from 0% to 0.5%. Hence, the highest and lowest porosities were found in W0-1.5 and W0.5–0, respectively.

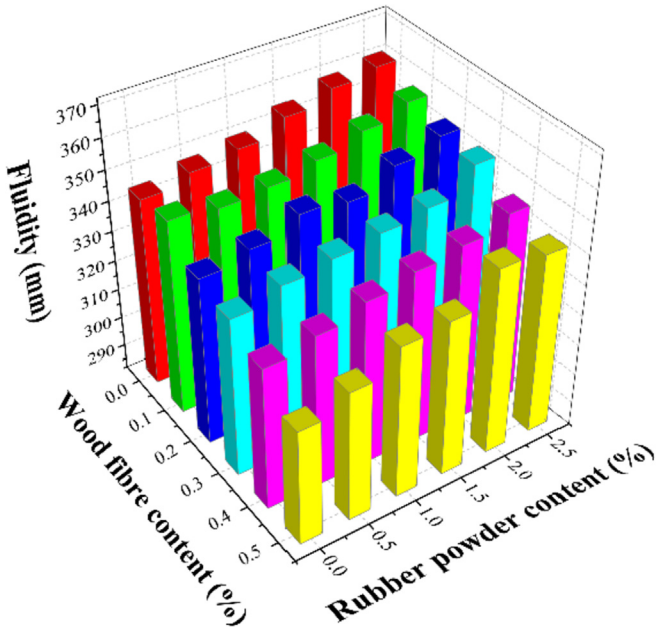

Fig. 2. Relationship between the fluidity of the slurry and rubber powder content.

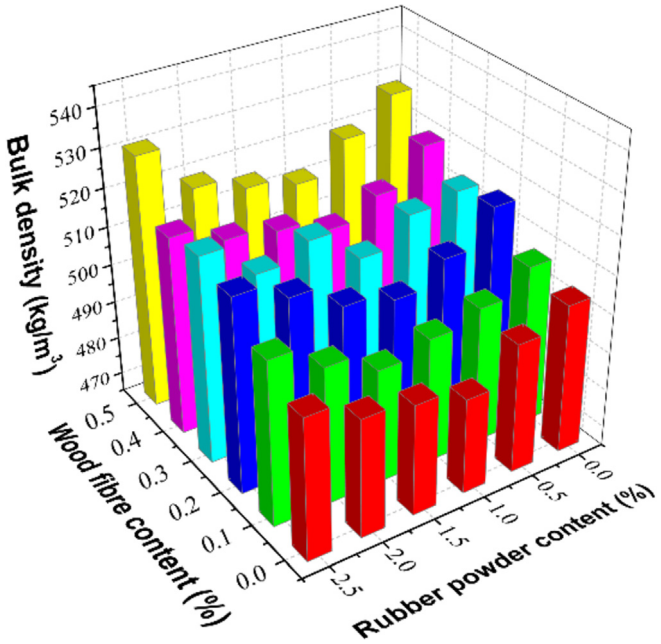

Fig. 3. Relationship between bulk density and rubber powder content.

Table 2
Porosity of samples.

Rubber powder content (%)	Porosity (%)					
	W0	W0.1	W0.2	W0.3	W0.4	W0.5
0.0	77.65	77.48	77.17	77.22	77.02	76.75
0.5	77.87	77.69	77.61	77.35	77.28	76.94
1.0	78.22	77.91	77.69	77.58	77.44	77.33
1.5	78.13	77.94	77.58	77.19	77.35	77.26
2.0	77.93	77.76	77.45	77.31	77.31	77.02
2.5	77.71	77.55	77.22	76.97	77.08	76.69

The surface macropores of W0-0, W0.4–0, W0-1.0, and W0.4–1.0 are shown in Fig. 4. Only surface macropores (in white) are shown in the figures. Owing to the effect of the rubber powder, the pores of W0-1.0 and W0.4–1.0 (Fig. 4c and d) seem to be slightly larger than those of W0-0 and W0.4–0 (Fig. 4a and b). According to calculation, the average macropore diameters were 1.274 mm for W0-0, 0.961 mm for W0.4–0, 0.133 mm for W0-1.0 and 1.297 mm for W0.4–1.0, respectively. Moreover, W0-1.0 and W0.4–1.0 have a more even gas pore distribution and smaller pores than do W0-0 and W0.4–0. The friction force between the wood fibre and the slurry affected the rheology of the slurry during the gas-generating process, which causes this change of pore structure.

3.3. Compressive and flexural strength

A three-dimensional (3D) colour surface map was created to better observe the variation in the compressive strength of AAC (Fig. 5). As the wood fibre content increased, the compressive strength increased and then decreased. Overall, adding wood fibre improved the compressive strength of AAC. When the rubber powder content remained the same, the compressive strength of all wood fibre-reinforced specimens was greater than that of

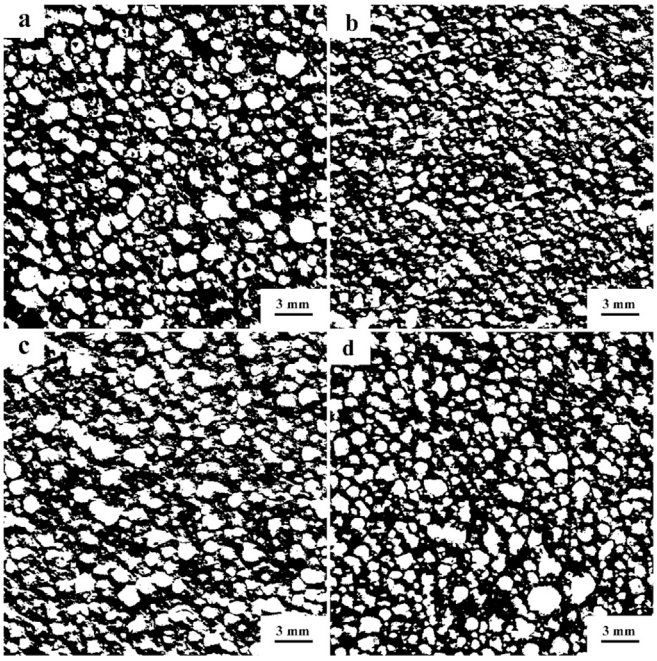

Fig. 4. Computer-processed images of the surface macropores of (a) W0-0, (b) W0.4–0, (c) W0-1.0, and (d) W0.4–1.0.

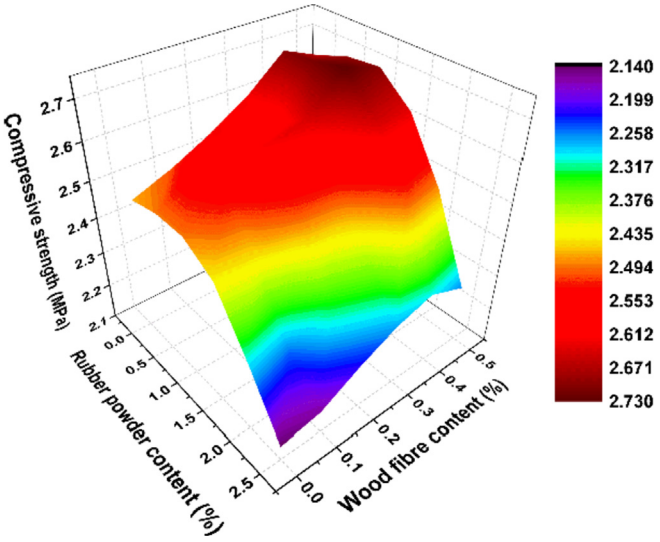

Fig. 5. 3D colour surface map showing the variation in compressive strength.

specimens without wood fibre. Moreover, the maximum compressive strength, obtained by W0.4–1.0, was about 1.09 times greater than that of W0-0. A similar increase in compressive strength of AAC was reported while basalt fibre was added in (Laukaitis et al., 2009).

The compressive strength increased slightly when the rubber powder content changed from 0% to 1.0%, indicating that a small amount of rubber powder had a positive effect on compressive strength. For example, the compressive strength of W0.4–1.0 was 0.02 MPa higher than that of W0.4–0. Because it is an elastic material, rubber powder under compression can absorb some energy. This may have caused the increase in compressive strength. However, a significant decrease in compressive strength was observed when the rubber powder content exceeded 1.0%. The compressive strengths of W0-2.5 and W0.4–2.5 were 13.4% and 14.8% less than those of W0-0 and W0.4–0, respectively. The large rubber powder content may have resulted in additional weak rubber powder-AAC matrix surfaces, which would have had a negative effect on compressive strength.

Fig. 6 is the 3D colour surface map that shows the variation of the flexural strength of AAC with different wood fibre and rubber powder contents. The effect of wood fibre on flexural strength was much more pronounced than the slight enhancement it made to compressive strength, and the same phenomenon was observed in previous studies (Laukaitis et al., 2012; Pehlivanlı et al., 2016). This significant increase may be attributed to the arrest of crack growth and energy transfer by the fibres, depending on their bond strength and properties (Abbass et al., 2018). For specimens without rubber powder, the flexural strength increased by 49% as the wood fibre content increased from 0% to 0.4%, that is, the toughness of AAC was significantly improved with the addition of wood fibre. However, the flexural strength decreased significantly when the wood fibre content changed from 0.4% to 0.5%, as did the compressive strength. A possible explanation for this decrease could be that the dispersivity of the wood fibre was important to its reinforcing effect on mechanical strength (Chuang et al., 2017; Lavagna et al., 2018). Excess wood fibre could not disperse evenly in the slurry because of the interference among the fibres, which led to an undesirable wood fibre distribution. Consequently, the additional weak fibre-fibre and fibre-AAC matrix interfaces were introduced. When a load was applied to these specimens, the stress in the specimens was redistributed, concentrating at the weak interfaces. Therefore, the mechanical strength of AAC decreased when the wood fibre was excessive.

Unlike the compressive strength, there was a slight decrease in the flexural strength as the rubber powder content increased from 0% to 1.0%. The flexural strength of W0-1.0 and W0.4–1.0 was 0.2 and 0.1 MPa lower than that of W0-0 and W0.4–0. In addition, the flexural strength sharply decreased as the rubber powder content increased from 1.0% to 2.5%. Compared with W0-1.0 and W0.4–1.0, the flexural strengths of W0-2.5 and W0.4–2.5 decreased by 26.3% and 31%, respectively. Because the weak rubber powder-AAC matrix surface was more vulnerable and sensitive under the stress from bending, leading to the significant decrease in flexural strength.

From the mechanical performances, it was concluded that the

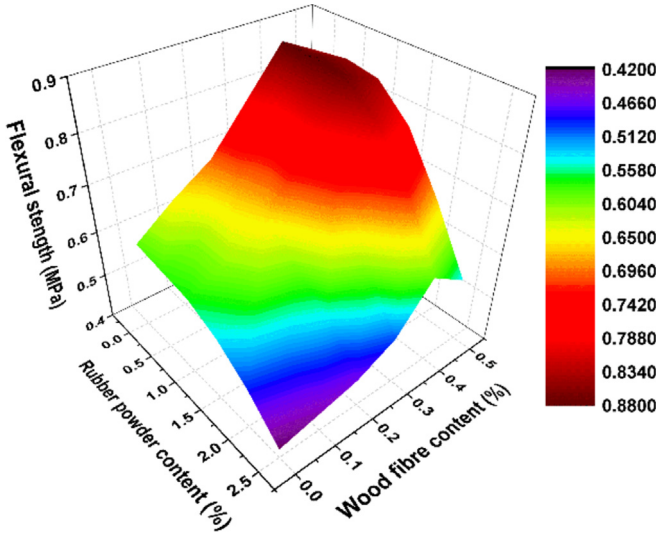

Fig. 6. 3D colour surface map showing the variation in flexural strength.

optimal wood fibre content was 0.4%. In addition, the low rubber powder content had almost no impact on the mechanical performance of AAC; therefore, the AAC could have 0.5% and 1.0% rubber powder content without any obvious decrease in its mechanical properties.

3.4. Thermal conductivity

Excellent thermal insulation is the most important property of AAC. Generally, the thermal conductivity of AAC is as much as 10 times lower than that of ordinary concrete (Asadi et al., 2018). The thermal conductivity of AAC is mainly a function of its density, porosity, pore size distribution, moisture content, and phase composition (Różycka and Pichór, 2016b). In addition, previous research reported that macropores were the main factor that affects thermal conductivity (Yuan et al., 2017). Under the same testing conditions, the effect of moisture content may not be prominent.

Base on the mechanical strengths analysis, it was sense to investigate the effect of rubber powder on the thermal insulation performance of specimens with 0.4 wood fibre content. Fig. 7 shows the relationship between thermal conductivity and rubber powder content. It was found that the thermal conductivity (the standard deviation ≤ 0.01 W/(m•K)) of AAC increased because of the addition of wood fibre, which was consistent with the experimental results in literature (Pehlivanlı et al., 2016). The thermal conductivity of W0.4–0 was 13.7% greater than that of W0-0. This increase could be explained by the smaller macropores and slightly lower porosity of W0.4–0.

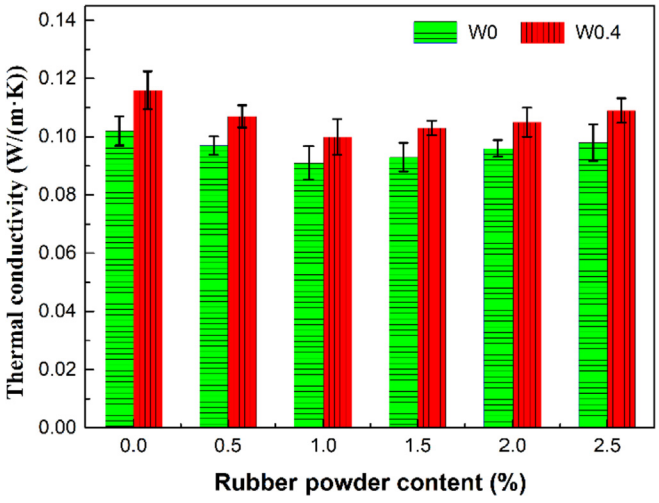

Fig. 7. Relationship between thermal conductivity and rubber powder content.

As presented in Fig. 7, all the thermal conductivities of the W0 and W0.4 specimens with rubber powder were smaller than those of the specimens without rubber powder (W0-0 and W0.4–0). It may conclude that rubber powder additive had a positive effect on the thermal conductivity of AAC. Moreover, the thermal conductivity decreased while rubber powder content increased from 0 to 1.0%. Compared with W0.4–0, the thermal conductivity of W0.4–1.0 decreased by 13.8%. The decrease mainly caused by the following two reasons. The air entrained by rubber powder increased the porosity of AAC, and rubber powder has a relatively low thermal conductivity, which would directly cause a decrease in the thermal conductivity of AAC. However, instead of entraining more air, excess rubber powder filled the pores and caused a decrease in porosity. Therefore, the thermal conductivity increased when the rubber powder content was large.

3.5. Energy-saving aspect

To investigate the effect of rubber powder on the energy-conserving property of AAC during heating and cooling cycles, the outer and inner surface temperatures were recorded and are displayed in Fig. 8.

The curves for the outdoor surface temperature are nearly superimposed. In the heating stage, the outer surface temperature increased rapidly and then reached a steady state. The rate of increase and the steady-state temperatures of the samples were almost the same. In addition, the outer surface temperature quickly decreased to room temperature in the cooling stage. The similar outer surface temperature results for the three samples demonstrated that the heat source device was stable.

Compared with the outer surface temperature, the inner surface temperature did not vary much. In the heating stage, the inner surface temperature reached the steady state about 80 min later than that of the outer surface temperature. The differences between the inner and outer surface temperatures were considerable, together with a very low cooled rate of the inner surface temperature, indicating the good thermal insulation resistance of AAC.

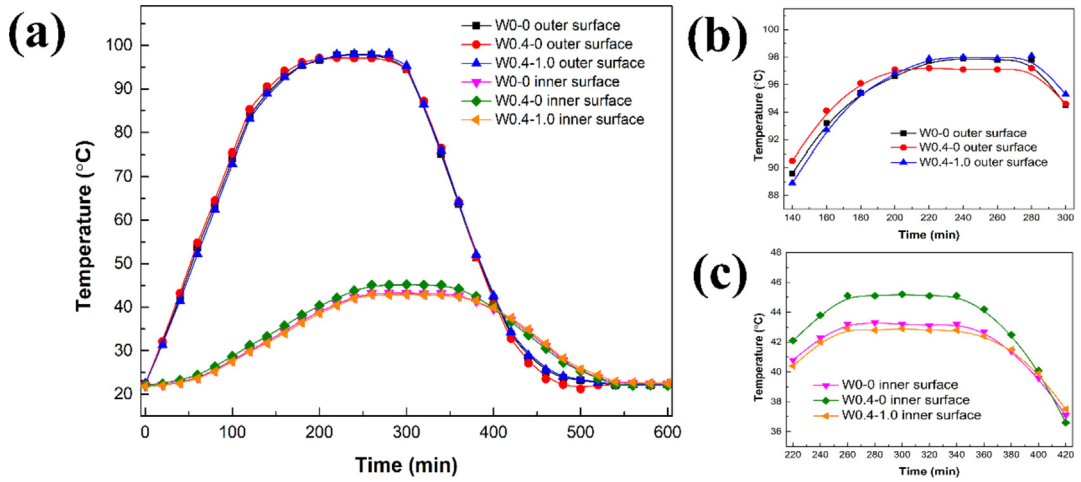

Fig. 8. Simulated outer and inner surface temperatures for the effect of rubber powder on the thermal insulation property, (b) steady state of outer surface temperature and (c) steady state of inner surface temperature.

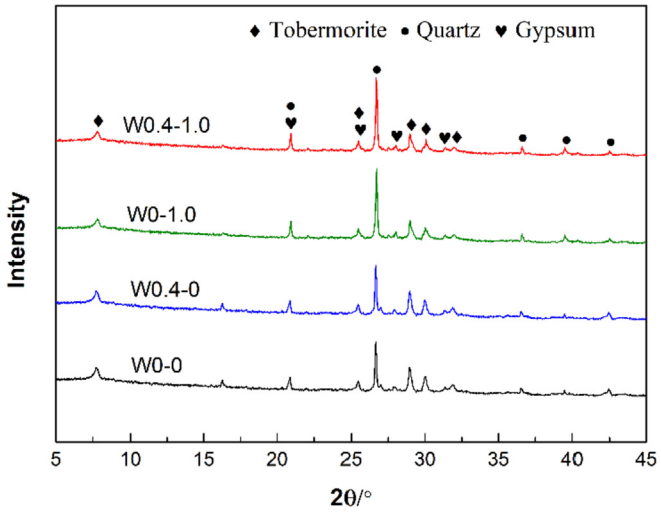

Fig. 9. XRD patterns of W0-0, W0.4–0, W0-1.0, and W0.4–1.0 specimens.

Compared with W0-0 and W0.1–1.0, a more obvious change in the inner surface temperature of W0.4–0 was observed. It indicated that wood fibre additive had a negative impact on the thermal insulation stability of AAC. As presented in Fig. 8c, W0.4–1.0 had the lowest steady-state inner surface temperature in the heating stage, followed by W0-0 and W0.4–0. The steady-state inner surface temperature of W0.4–1.0 was about 2.2 °C lower than that of W0.4–0, meaning that less energy would be consumed to maintain room temperature (Cerón et al., 2011). According to the endothermic and exothermic formula, it took more than 2800 J of energy to reduce the temperature of one cubic meter of air by 2.2 °C. This satisfactory results were attributed to the improvement on the thermal insulation performance caused by rubber powder. Moreover, the inner surface temperature curves of W0-0 and W0.4–1.0 were nearly overlapped, which meant the equivalent thermal insulation properties of W0-0 and W0.4–1.0.

Thus, rubber powder, especially 1.0% content, can be used to reduce or eliminate the negative effect of wood fibre on the thermal insulation property of AAC.

3.6. Phase components and microstructure

XRD analyses were performed to investigate the mineral phase components in the AAC samples. The diffraction patterns of W0-0, W0.4–0, W0-1.0, and W0.4–1.0 specimens presented in Fig. 9 show that the major mineral phases in all the specimens were nearly the same. Peaks for tobermorite, quartz, and gypsum were clearly observed in all samples. From this, one can conclude that the toughening and strengthening of AAC caused by wood fibre was a physical interaction, not a chemical one, and that the slight increase in the compressive strength of W0-1.0 and W0.4–1.0 was due to the physical property of rubber powder, as mentioned before.

An important index in XRD analyses is the specific intensity, which is strongly influenced by product content. There was little difference between the peak specific intensities of W0-0 and W0.4–0 and of W0-1.0 and W0.4–1.0. The diffraction peaks of tobermorite were slightly weaker in W0-1.0 and W0.4–1.0 than in W0-0 and W0.4–0. Fig. 9 clearly shows that the intensity of quartz was enhanced in W0-1.0 and W0.4–1.0. These variations in specific peak intensity may be the result of rubber powder impeding the chemical reactions during AAC preparation. Furthermore, the relatively high thermal conductivity coefficient of residual quartz may cause the deterioration of the thermal property of AAC. On the other hand, the thermal conductivity coefficient decreased when rubber powder was added to AAC. The change in pore structure caused by the rubber powder additive may explain this contradictory phenomenon.

SEM micrographs of the microstructure of W0-0 and W0.4–1.0 specimens are presented in Fig. 10. It was reported that the microstructure of AAC depended on the type, amount, and phase composition of the constituent materials (Różycka and Pichór, 2016a). The plates of tobermorite, the main mineral phase in both

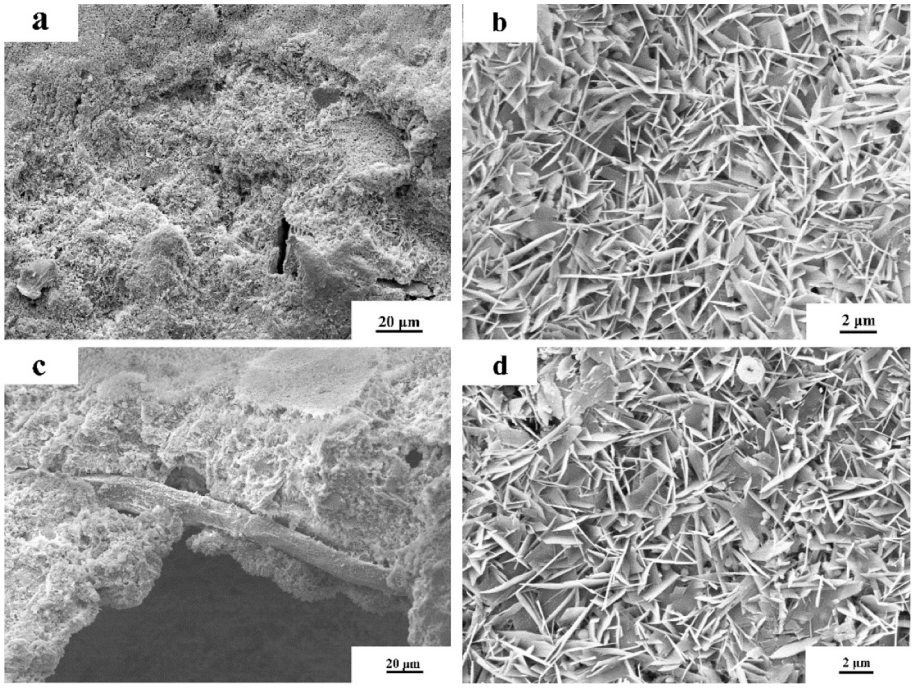

Fig. 10. SEM micrographs of (a, b) the W0-0 specimen and (c, d) the W0.4–1.0 specimen.

samples, connected and overlapped with each other to form a firm skeleton. W0-0 and W0.4–1.0 have similar microstructures, meaning that wood fibre and rubber powder did not cause extra chemical reactions.

Some hydration products were adsorbed onto the rough surface of the wood fibre. Bent soft wood fibre can be seen in the AAC matrix shown in Fig. 10c. This bending could increase the mechanical interaction between the wood fibre and the AAC matrix. In addition, some residual quartz crystals are observed in Fig. 10d, consistent with the XRD analyses.

4. Conclusions

Different contents of rubber powder and wood fibre, produced from solid waste, were used to prepare high-performance AAC. The fluidity of the slurry, bulk density, pore structure, mechanical properties, thermal properties, phase composition, and microstructure of the AAC specimens were systematically investigated. On the basis of results presented in this paper, following conclusions were drawn:

The mechanical properties of AAC were significantly enhanced with the addition of wood fibre, especially its flexural strength. With respect to the mechanical strengths of AAC, The wood fibre content of 0.4% was found to be the optimal content.

Rubber powder had a positive impact on the pore structure of AAC because of the characteristic of air entrainment, resulting in the satisfactory improvement in the thermal insulation property of AAC including thermal conductivity and energy saving aspect. Moreover, rubber powder contents of 0.5% and 1.0% had almost no effect on the mechanical performance of AAC.

High-performance AAC could be obtained with the simultaneous addition of 1.0% rubber powder and 0.4% wood fibre. And the analyses of XRD and SEM revealed that the modifying effects of wood fibre and rubber powder on AAC were physical functions.

Acknowledgments

This work was supported by the National Natural Science Foundation of China (grant NO. 51674184).

References

Abbass, W., Khan, M.I., Mourad, S., 2018. Evaluation of mechanical properties of steel fiber reinforced concrete with different strengths of concrete. Constr. Build. Mater. 168, 556–569.
Asadi, I., Shafigh, P., Abu Hassan, Z.F.B., Mahyuddin, N.B., 2018. Thermal conductivity of concrete – a review. J. Build. Eng. 20, 81–93.
Ashish, D.K., 2018. Feasibility of waste marble powder in concrete as partial substitution of cement and sand amalgam for sustainable growth. J. Build. Eng. 15, 236–242.
Aslani, F., Ma, G., Yim Wan, D.L., Tran Le, V.X., 2018. Experimental investigation into rubber granules and their effects on the fresh and hardened properties of self-compacting concrete. J. Clean. Prod. 172, 1835–1847.
Blankenhorn, P.R., Blankenhorn, B.D., Silsbee, M.R., Dicola, M.J.C., Research, C., 2001. Effects of fiber surface treatments on mechanical properties of wood fiber–cement composites, 31 (7), 1049–1055.
Bonakdar, A., Babbitt, F., Mobasher, B., 2013. Physical and mechanical characterization of fiber-reinforced aerated concrete (FRAC). Cement Concr. Compos. 38, 82–91.
Cao, V.D., Pilehvar, S., Salas-Bringas, C., Szczotok, A.M., Rodriguez, J.F., Carmona, M., Al-Manasir, N., Kjøniksen, A.-L., 2017. Microencapsulated phase change materials for enhancing the thermal performance of Portland cement concrete and geopolymer concrete for passive building applications. En. Conv. Manag. 133, 56–66.
Cerón, I., Neila, J., Khayet, M., 2011. Experimental tile with phase change materials (PCM) for building use. En. Build. 43 (8), 1869–1874.
Cheng, X.W., Huang, S., Guo, X.Y., Duan, W.H., 2017. Crumb waste tire rubber surface modification by plasma polymerization of ethanol and its application on oil-well cement. Appl. Surf. Sci. 409, 325–342.
China Building Energy Saving Technic Association, 2019. Research report on building energy consumption of China in 2018. Industry 2, 26–31.
Chuang, W., Geng-sheng, J., Bing-liang, L., Lei, P., Ying, F., Ni, G., Ke-zhi, L., 2017. Dispersion of carbon fibers and conductivity of carbon fiber-reinforced cement-based composites. Ceram. Int. 43 (17), 15122–15132.
Cong, X.Y., Lu, S., Yao, Y., Wang, Z., 2016. Fabrication and characterization of self-ignition coal gangue autoclaved aerated concrete. Mater. Des. 97, 155–162.
Dobrotă, D., Dobrotă, G., 2018. An innovative method in the regeneration of waste rubber and the sustainable development. J. Clean. Prod. 172, 3591–3599.
El-Didamony, H., Amer, A.A., Mohammed, M.S., El-Hakim, M.A., 2019. Fabrication and properties of autoclaved aerated concrete containing agriculture and industrial solid wastes. J. Build. Eng. 22, 528–538.
Faraca, G., Boldrin, A., Astrup, T., 2019. Resource quality of wood waste: the importance of physical and chemical impurities in wood waste for recycling. Waste Manag. 87, 135–147.
Ferretti, D., Michelini, E., Rosati, G., 2015. Cracking in autoclaved aerated concrete: experimental investigation and XFEM modeling. Cement Concr. Res. 67, 156–167.
He, T., Xu, R., Chen, C., Yang, L., Yang, R., Da, Y., 2018. Carbonation modeling analysis on carbonation behavior of sand autoclaved aerated concrete. Constr. Build. Mater. 189, 102–108.
Hijazi, A., Boyadjian, C., Ahmad, M.N., Zeaiter, J., 2018. Solar pyrolysis of waste rubber tires using photoactive catalysts. Waste Manag. 77, 10–21.
Hossain, M.U., Poon, C.S., 2018. Comparative LCA of wood waste management strategies generated from building construction activities. J. Clean. Prod. 177, 387–397.
Ismail, M.K., Sherir, M.A.A., Siad, H., Hassan, A.A.A., Lachemi, M., 2018. Properties of self-consolidating engineered cementitious composite modified with rubber. J. Mater. Civ. Eng. 30 (4), 9.
Israngkura Na Ayudhya, B., 2016. Comparison of compressive and splitting tensile strength of autoclaved aerated concrete (AAC) containing water hyacinth and polypropylene fibre subjected to elevated temperatures. Mater. Struct. 49 (4), 1455–1468.
Kahwaji, S., Johnson, M.B., Kheirabadi, A.C., Groulx, D., White, M.A., 2018. A comprehensive study of properties of paraffin phase change materials for solar thermal energy storage and thermal management applications. En 162, 1169–1182.
Kočí, V., Maděra, J., Černý, R., 2013. Computer aided design of interior thermal insulation system suitable for autoclaved aerated concrete structures. Appl. Therm. Eng. 58 (1), 165–172.
Koudelka, T., Kruis, J., Maděra, J., 2015. Coupled shrinkage and damage analysis of autoclaved aerated concrete. Appl. Math. Comput. 267, 427–435.
Krishna, N.K., Prasanth, M., Gowtham, R., Karthic, S., Mini, K.M., 2018. Enhancement of properties of concrete using natural fibers. Mater. Today: SAVE Proc. 5, 23816–23823 (11, Part 3).
Laukaitis, A., Kerienė, J., Kligys, M., Mikulskis, D., Lekūnaitė, L., 2012. Influence of mechanically treated carbon fibre additives on structure formation and properties of autoclaved aerated concrete. Constr. Build. Mater. 26 (1), 362–371.
Laukaitis, A., Kerienė, J., Mikulskis, D., Sinica, M., Sezemanas, G., 2009. Influence of fibrous additives on properties of aerated autoclaved concrete forming mixtures and strength characteristics of products. Constr. Build. Mater. 23 (9), 3034–3042.
Lavagna, L., Musso, S., Ferro, G., Pavese, M., 2018. Cement-based composites containing functionalized carbon fibers. Cement Concr. Compos. 88, 165–171.
Li, M., Qian, X.Y., Peng, H., Wu, Z.S., 2017. The influence of silicon dioxide nanoparticles on microstructure and properties of autoclaved aerated concrete. Cem. Wapn. Bet. 22 (4), 320–327.
Long, W.J., Li, H.D., Wei, J.J., Xing, F., Han, N.X., 2018. Sustainable use of recycled crumb rubbers in eco-friendly alkali activated slag mortar: dynamic mechanical properties. J. Clean. Prod. 204, 1004–1015.
Ma, B.-g., Cai, L.-x., Li, X.-g., Jian, S.-w., 2016. Utilization of iron tailings as substitute in autoclaved aerated concrete: physico-mechanical and microstructure of hydration products. J. Clean. Prod. 127, 162–171.
Nasser, R.A., Salem, M.Z.M., Al-Mefarrej, H.A., Aref, I.M., 2016. Use of tree pruning wastes for manufacturing of wood reinforced cement composites. Cement Concr. Compos. 72, 246–256.
Noumowe, A.J.C., Research, C., 2005. Mechanical properties and microstructure of high strength concrete containing polypropylene fibres exposed to temperatures up to 200. °C 35 (11), 2192–2198.
Pehlivanlı, Z.O., Uzun, İ., Demir, İ., 2015. Mechanical and microstructural features of autoclaved aerated concrete reinforced with autoclaved polypropylene, carbon, basalt and glass fiber. Constr. Build. Mater. 96, 428–433.
Pehlivanlı, Z.O., Uzun, İ., Yücel, Z.P., Demir, İ., 2016. The effect of different fiber reinforcement on the thermal and mechanical properties of autoclaved aerated concrete. Constr. Build. Mater. 112, 325–330.
Quiroga, A., Marzocchi, V., Rintoul, I., 2016. Influence of wood treatments on mechanical properties of wood–cement composites and of Populus Euro-americana wood fibers. Compos. B Eng. 84, 25–32.
Rahimi, R.S., Nikbin, I.M., Allahyari, H., Habibi, T.S., 2016. Sustainable approach for recycling waste tire rubber and polyethylene terephthalate (PET) to produce green concrete with resistance against sulfuric acid attack. J. Clean. Prod. 126, 166–177.
Ramdani, S., Guettala, A., Benmalek, M.L., Aguiar, J.B., 2019. Physical and mechanical performance of concrete made with waste rubber aggregate, glass powder and silica sand powder. J. Build. Eng. 21, 302–311.
Różycka, A., Pichór, W., 2016a. Effect of perlite waste addition on the properties of autoclaved aerated concrete. Constr. Build. Mater. 120, 65–71.
Różycka, A., Pichór, W., 2016b. Effect of perlite waste addition on the properties of

autoclaved aerated concrete. Constr. Build. Mater. 120, 65–71.
Schreiner, J., Jansen, D., Ectors, D., Goetz-Neunhoeffer, F., Neubauer, J., Volkmann, S., 2018. New analytical possibilities for monitoring the phase development during the production of autoclaved aerated concrete. Cement Concr. Res. 107, 247–252.
Sheng, Y., Li, H., Geng, J., Tian, Y., Li, Z., Xiong, R., 2017. Production and performance of desulfurized rubber asphalt binder. Int. J. Pav. Res. and Techn. 10 (3), 262–273.
Sienkiewicz, M., Janik, H., Borzędowska-Labuda, K., Kucińska-Lipka, J., 2017. Environmentally friendly polymer-rubber composites obtained from waste tyres: a review. J. Clean. Prod. 147, 560–571.
Sofi, A., 2018. Effect of waste tyre rubber on mechanical and durability properties of concrete – a review. Ain Shams Eng. J. 9 (4), 2691–2700.
Souza, A.M., Nascimento, M.F., Almeida, D.H., Lopes Silva, D.A., Almeida, T.H., Christoforo, A.L., Lahr, F.A.R., 2018. Wood-based composite made of wood waste and epoxy based ink-waste as adhesive: a cleaner production alternative. J. Clean. Prod. 193, 549–562.
Straub, C., Florea, M.V.A., Brouwers, H.J.H., 2015. Autoclaved Aerated Concrete : Mix Parameters and Their Influence on Final Properties.
Thomas, B.S., Gupta, R.C., 2016. A comprehensive review on the applications of waste tire rubber in cement concrete. Ren. Sust. En. Rev. 54, 1323–1333.
Thomas, B.S., Gupta, R.C., Panicker, V.J., 2016. Recycling of waste tire rubber as aggregate in concrete: durability-related performance. J. Clean. Prod. 112, 504–513.
Usman, M., Khan, A.Y., Farooq, S.H., Hanif, A., Tang, S., Khushnood, R.A., Rizwan, S.A., 2018. Eco-friendly self-compacting cement pastes incorporating wood waste as cement replacement: a feasibility study. J. Clean. Prod. 190, 679–688.
Wang, L., Yu, I.K.M., Tsang, D.C.W., Li, S., Li, J.-s., Poon, C.S., Wang, Y.-S., Dai, J.-G., 2017. Transforming wood waste into water-resistant magnesia-phosphate cement particleboard modified by alumina and red mud. J. Clean. Prod. 168, 452–462.
Wang, L., Yu, I.K.M., Tsang, D.C.W., Yu, K., Li, S., Sun Poon, C., Dai, J.-G., 2018. Upcycling wood waste into fibre-reinforced magnesium phosphate cement particleboards. Constr.and Build. Mater. 159, 54–63.
Wang, X., Feng, W., Cai, W.G., Ren, H.,, Ding, C., Zhou, N., 2019. Do residential building energy efficiency standards reduce energy consumption in China? – a data-driven method to validate the actual performance of building energy efficiency standards. En. Pol. 131.
Xargay, H., Folino, P., Nuñez, N., Gómez, M., Caggiano, A., Martinelli, E., 2018. Acoustic emission behavior of thermally damaged self-compacting high strength fiber reinforced concrete. Constr. Build. Mater. 187, 519–530.
Yang, C., Matalkah, F., Weerasir, R.R., Balachandra, A., Soroushian, P.J.C.I., 2017. Dispersion of Fibers in Ultra-high-performance Concrete, pp. 53–58 (December).
Yuan, B., Straub, C., Segers, S., Yu, Q.L., Brouwers, H.J.H., 2017. Sodium carbonate activated slag as cement replacement in autoclaved aerated concrete. Ceram. Int. 43 (8), 6039–6047.
Zhang, X., Sinha, T.K., Lee, J., Ahn, Y., Kim, J.K., 2019. Temperature dependent amphoteric behavior of Bis[3-(triethoxysilyl)propyl]tetrasulfide towards recycling of waste rubber: a triboelectric investigation. J. Clean. Prod. 213, 569–576.
Zhu, J., Zhang, X., Liang, M., Lu, C., 2011. Enhancement of processability and foamability of ground tire rubber powder and LDPE blends through solid state shear milling. J. Polym. Res. 18 (4), 533–539.